energy&fuels

Article

Molecular Characterization of Strongly and Weakly Interfacially Active Asphaltenes by High-Resolution Mass Spectrometry

Dewi A. Ballard, Martha L. Chacón-Patiño, Peiqi Qiao, Kevin J. Roberts, Robert Rae, Peter J. Dowding, Zhenghe Xu, and David Harbottle*

Cite This: *Energy Fuels* 2020, 34, 13966−13976

Read Online

ACCESS | Metrics & More | Article Recommendations | Supporting Information

ABSTRACT: Asphaltenes are a complex mixture of molecular structures with a variety of functionalities, which in turn impacts their physical properties. Discriminating between asphaltenes that are strongly and weakly interfacially active is providing a new direction to mitigate asphaltene-related problems. Whole asphaltenes (WA) were extracted from a South American heavy crude oil, further fractionated into interfacially active asphaltenes (IAA) and remaining asphaltenes (RA), and molecularly characterized by positive-ion (+) atmospheric pressure photoionization (APPI) using a 9.4 T Fourier transform ion cyclotron mass spectrometer (FT-ICR MS). The IAA fraction was found to contain a greater abundance of heteroatoms with >50% of IAA containing two or more heteroatoms as compared to ∼30% for RA. The IAA fraction was enriched in oxygen-containing species, more specifically higher-order O_x and O_xS_y groups that were predominantly of low DBE. Gas-phase fragmentation of RA and IAA precursor ions (m/z 650) by infrared multiphoton dissociation (IRMPD) revealed an abundance of multi-core motifs in IAA, while RA was found to be a mixture of single-core and multi-core structures. Analysis of the fragmented ions showed a prevalence of nitrogen-containing species of high DBE (aromatic molecular structures), while oxygen-containing species were most likely associated with aliphatic side chains. Extrography fractionation of RA and IAA verified the abundance of multi-core motifs in IAA, which were highly polar and of low DBE and carbon number. These "atypical" structures of IAA are classified as asphaltenes as a result of their functionality and polarity rather than high aromaticity.

INTRODUCTION

Asphaltenes are defined as the fraction of crude oil soluble in aromatic solvents and insoluble in *n*-alkanes,[1−3] with the molecular structure often described by a single polycyclic aromatic core with alkyl-side chains. This structure is frequently described as *island*-like, but for the purpose of clarity, we refer to this structure as single-core. Asphaltenes have also been found to contain multiple aromatic cores connected by covalent bonds such as aryl−aryl or alkyl-chains, which are typically referred to as *aryl*-linked and *archipelago*-like structures.[4,5] This type of structure we refer to as multi-core. Asphaltenes are reported to have a hydrogen-to-carbon (H/C) ratio between ∼0.90 and 1.20 and contain several heteroatoms such as sulfur, oxygen, and nitrogen (total content between ∼5 and 10 wt %) and trace amounts of metals (vanadium and nickel).[6,7] While asphaltenes are frequently studied, it is increasingly clear that the behavior of asphaltenes in the bulk fluid and at interfaces (solid−liquid and liquid−liquid) is greatly influenced by the asphaltene chemistry and molecular structure.

Fractionating asphaltenes into smaller subgroups provides greater clarity on their physicochemical properties. Step-wise fractionation of asphaltenes is most commonly achieved by decreasing the solvent aromaticity to increase alkane content, preferentially precipitating progressively less soluble asphaltenes. By comparing the chemistry of precipitated and soluble asphaltenes from four different crude oils, Spiecker et al.[8] found only marginal differences in composition among the four crude oils, with the precipitated fractions being slightly more aromatic with slightly higher nitrogen and oxygen contents. Changes in sulfur content between the two asphaltene fractions were found to be negligible. The most discernible changes were in the metal contents, with the precipitated fractions being more enriched in Fe, Ni, and V.

Crude oils that exhibit severe deposition problems have been found to contain higher amounts of polarizable compounds.[9] By comparing the asphaltene subfractions obtained via adsorption on $CaCO_3$, Pinto et al.[10] observed more distinct changes in the elemental composition: adsorbed asphaltenes showed higher contents of oxygen-containing compounds and decreased alkyl-substitution as compared with whole asphaltenes and weakly adsorbed fractions. Kilpatrick et al. confirmed that the asphaltene fraction stabilizing water-in-oil emulsions was more polar and acidic (higher oxygen content) and of lower double bond equivalents (DBE = total number of rings and double bonds involving carbon).[11,12] These authors found that the stabilizing asphaltene fraction formed larger asphaltene aggregates and formed stronger bonds,[11] as evidenced by neutron scattering and interfacial rheology measurements.[8,12,13] Following the method of Wu,[14] Czarnecki and co-workers[15−17]

separated the interfacial material from crude oils and asphaltenes. Their study revealed an abundance of compounds of low aromaticity being enriched in O_x and O_xS_y groups (S- and O-containing functionalities) and being depleted in N-containing functionalities. Such characteristics were also found for asphaltenes adsorbed onto calcium carbonate.[18−20]

Further fractionation of asphaltenes from both bitumen and heavy oil by the E-SARA method[21−25] has revealed differences in the size and shape of asphaltene nanoaggregates, which correlate to the asphaltene chemistry. The emulsion stabilizing asphaltenes, referred to as interfacially active asphaltenes (IAA), account for only ∼2 wt % of the whole asphaltenes (WA); the remaining, less interfacially active asphaltenes are referred to as remaining asphaltenes (RA). Chemical characterization of the IAA and RA fractions revealed differences in chemical composition, with sulfur and oxygen contents in the IAA fraction exceeding those in RA.[24,25] More significantly, the abundance of different functional groups, in particular the presence of sulfoxides as a strong hydrogen-bond acceptor in IAA, contributes to the strong stabilizing (emulsion stability) potential of the IAA fraction. Recently, SANS measurements of WA extracted from bitumen and heavy oil revealed a remarkable similarity in asphaltene nanoaggregates size and shape, even though the contents of heteroatoms varied significantly.[23] However, comparing IAA and RA extracted from heavy oil, similar differences in the heteroatom (sulfur and oxygen) content were observed but, crucially, the IAA fraction was enriched in sulfoxide and carbonyl groups. The higher concentration of sulfoxide groups in IAA was postulated to govern the nanoaggregate size and shape, with the IAA nanoaggregates being substantially larger and more porous than RA.[23] The SANS study highlighted the possibility that the two asphaltene fractions, IAA and RA, aggregate differently, with the mechanism likely dependent on the chemistry of asphaltenes.

Although the presence of sulfoxides in crude oils has been widely debated,[26−30] such uncertainty has resulted from an inability to measure sulfoxide species. Using solvent extraction, Ren et al.[31] separated polar (sulfoxides) and nonpolar (sulfides and thiophenes) sulfur fractions from three different crude oils. The extracted samples were analyzed by Fourier transform-ion cyclotron resonance mass spectrometry (FT-ICR MS). The results showed a more significant abundance of the O_1S_1 class species in the polar fraction than in the nonpolar fraction. Reduction of the polar fraction by $LiAlH_4$ confirmed the species to be sulfoxides. The authors stated that the polar fraction of sulfur accounted for 27%−46% of the total sulfur, with only 0.8%−5.7% of the total sulfur being sulfoxides. Although the sulfoxide-to-total-sulfur content is relatively small, its presence and likely position within the asphaltene molecular structure appears to be a dominant feature governing the aggregation of asphaltene molecules.

Recent studies demonstrated that differences in aggregation tendency between structures may promote differences in ion production efficiency, which results in selective ionization of asphaltenes by atmospheric pressure photoionization (APPI).[32] To fully characterize asphaltenes, an extrography fractionation method was developed, in which asphaltenes adsorbed on SiO_2 were sequentially extracted using acetone, Heptol, and toluene/tetrahydrofuran/methanol (Tol/THF/MeOH). This fractionation method extracts condensed polyaromatic structures, nonpolar alkyl-aromatic compounds, and highly polarizable species, which interact most strongly with the silanol groups of

the silica gel.[32−34] Characterization by APPI FT-ICR MS and gas-phase fragmentation by infrared multi-photon dissociation revealed that the fraction extracted using acetone produced ∼50-fold more monomeric asphaltene ions (nonaggregated) of abundant single-core motifs. Conversely, the Tol/THF/MeOH compounds were more difficult to ionize and revealed abundant multi-core structures. These authors suggested a link between asphaltene aggregation and low ionization efficiency.

Despite extensive efforts to characterize asphaltenes, more detailed analysis of asphaltene subfractions, in particular those that strongly adsorb at interfaces, is needed to reveal determinant physicochemical properties that govern asphaltenes behaviors. High-resolution molecular characterization of asphaltenes is possible using positive-ion (+) atmospheric pressure photoionization (APPI) custom-built 9.4 T FT-ICR MS and is used for the first time to study RA and IAA fractions extracted from a South American heavy crude oil. The gas-phase fragmentation via IRMPD is also performed to understand the molecular structure of the most abundant asphaltene ion generated from each fraction.

■ MATERIALS AND METHODS

Samples and Chemicals. Whole asphaltenes (WA) were extracted from heavy oil (Llanos region, Colombia; API 13.6°) using a standard protocol for asphaltene precipitation.[25] Heavy oil (50 mL) was mixed with 1950 mL of n-heptane (Sigma-Aldrich) (40:1 by volume) in a 2000 mL beaker to precipitate asphaltenes. After 24 h, the diluted sample was filtered using an 8 μm Whatman #2 filter paper to collect the precipitated asphaltenes, which were then washed with excess n-heptane until the filtrate appeared clear. Precipitated asphaltenes were then dissolved in excess toluene (HPLC-grade, Sigma-Aldrich) to remove the fine mineral solids by centrifugation at 20 000g for 20 min. Asphaltenes were then dried under nitrogen, stored in airtight sealed glass vials, wrapped in aluminum foil, and refrigerated prior to their use. Prior to FT-ICR analysis, asphaltenes were further cleaned using heptane by Soxhlet extraction (Whatman, GE Healthcare, Little Chalfont, UK).

E-SARA. WA was fractionated into IAA and RA following the E-SARA separation method.[22] Deionized water (10 mL) was added to 100 mL of WA-in-toluene (10 g/L); the mixture was homogenized (T18 Ultra-Turrax, IKA) at 13 000 rpm for 15 min. The emulsion was gently agitated for 24 h and subsequently centrifuged at 11 000 rpm (Heraeus Megafuge 16 Centrifuge, ThermoFisher Scientific) to separate the asphaltene-stabilized water droplets from the continuous oil phase. The supernatant was then removed without disturbing the "emulsion cake", and an equal volume of fresh toluene was added and shaken to remove any loosely bound asphaltenes at the oil−water interface. Following six consecutive toluene washes, the emulsion droplets were transferred to a preweighed glass beaker and left for 12 h in a vacuum oven at 60 °C. This process is aimed to evaporate deionized water and the remaining solvent. Using this procedure, 1 g of WA heavy oil (asphaltene content of the heavy oil was ∼25 wt %) yielded ∼15 mg of IAA, confirming that the fraction of asphaltenes partitioned at the oil−water interface was ∼1.5 wt % of WA.

Extrography Fractionation. The RA and IAA fractions were further separated using the extrography method,[32] which assisted the selective separation of asphaltenes with a high production efficiency of nonaggregated ions in APPI (high monomer ion yield, MIY) to facilitate mass spectral characterization of difficult-to-ionize species. Asphaltenes were dissolved in dichloromethane (DCM, J.T. Baker) at 0.2 g/L and mixed for 1 h with chromatographic-grade silica gel (Fluka Analytical, 70−230 mesh, pore size 60 Å) at 5 mg of asphaltenes per 1 g of SiO_2 mass ratio. The mixture was completely dried under nitrogen (8 h) and then Soxhlet extracted with acetone for 24 h (HPLC-grade, J.T. Baker), separating species of high monomer ion yield, which typically bias mass spectrometry analyses of asphaltenes due to ion suppression. The mixture of the remnant asphaltenes + silica gel was again dried and
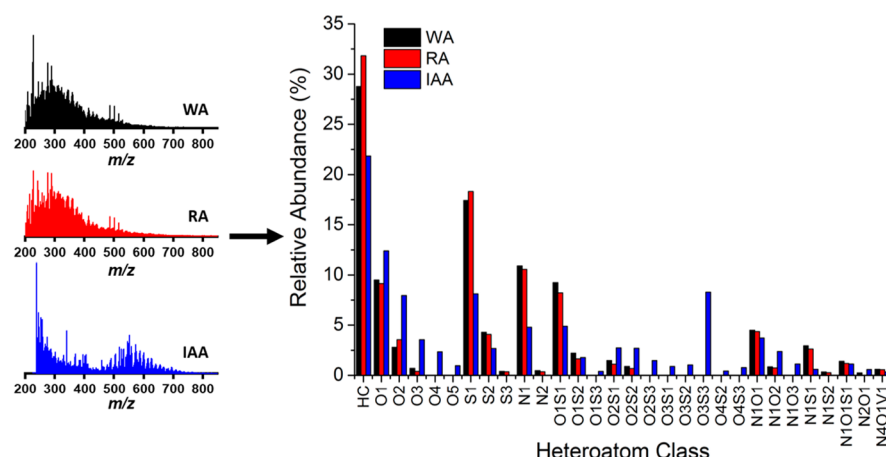
Figure 1. APPI(+) FT-ICR MS of WA, RA, and IAA extracted from a South American heavy oil (left), with the relative abundance (%) of assigned heteroatom classes for each of the three asphaltene samples (right).

Soxhlet extracted with Heptol (1:1 v/v n-heptane and toluene) to separate nonpolar alkyl-aromatic compounds.[35−37] A third extraction was conducted using a mixture of toluene, tetrahydrofuran (THF), and methanol (MeOH) in a volume ratio of 2:2:1 to extract the polarizable asphaltenes that interact with the silica gel via hydrogen bonding.[38−40] Yields for each extraction and monomer ion yields (MIY) are provided in Figure 6.

Positive-Ion Atmospheric Pressure Photoionization 9.4 T Fourier Transform Ion Cyclotron Resonance Mass Spectroscopy ((+)APPI 9.4 T FT-ICR MS) and Infrared multi-photon Dissociation (IRMPD). All asphaltene samples were diluted to 100 μg/mL in toluene (HPLC-grade, Sigma-Aldrich) and directly infused into a Thermo-Fisher Ion Max APPI source (Thermo-Fisher Scientific, Inc.)[41] at a vaporizer temperature of 350 °C and a sample flow rate of 50 μL/min. Sample nebulization was assisted by N_2 gas. Gas-phase neutrals were photoionized by 10.2 eV photons from a Krypton lamp. A custom-built 9.4-T Fourier transform ion cyclotron resonance mass spectrometer was used to characterize the ionized asphaltene species, with 100 scans averaged per sample.[42] The RA and WA samples were characterized over an m/z range of 200−1000, and the IAA sample was measured over an m/z range of 240−1000. For IAA, the removal of low m/z data was performed using a quadrupole mass filter to improve the signal of higher molecular weight compounds in the IAA sample, as a high abundance of low m/z ions derived from toluene clusters was detected. Due to the high abundance of low m/z ions derived from toluene clusters, the removal of low m/z data was performed using a quadrupole mass filter to improve the signal of higher molecular weight compounds in the IAA sample. Data collection was performed using a modular ICR data acquisition system (PREDATOR).[42−44] Positive ions were accumulated externally for 100−10000 ms in a radio frequency (rf)-only octopole and collisionally cooled with helium prior to transfer to a custom dynamically harmonized FT-ICR cell. One hundred time-domain acquisitions were coadded, Hanning-apodized, zero-filled, and Fourier transformed. Analysis software assisted frequency transformation to m/z by the quadrupolar electric trapping potential approximation, peak detection (>6σ baseline root-mean-square (RMS) noise), and internal calibration by extended homologous alkylation series. Molecular formula assignment and data visualization by iso-abundance-contoured plots of double bond equivalents (DBE) vs carbon number were obtained using the PetroOrg N-18.3 software.[45] Unless otherwise stated, the data is the combination of radical and protonated ions, with mass errors less than 0.2 ppm and root-mean-square errors below 0.14 ppm. The data was also processed to only contain ions following a homologous series of at least five and peaks identified to contain up to six sulfur, oxygen, and/or nitrogen atoms. The molecular formula assignment was performed using an iterative process, in which low-heteroatom content ions are assigned first to decrease the possibility of misassignments. The DBE is equal to the number of carbon involving rings and double bonds in a given structure

and is calculated from the assigned molecular formulas using the equation DBE $= C - \frac{H}{2} + \frac{N}{2} + 1$, where C is the number of carbon atoms, H is the number of hydrogens, and N is the number of nitrogen atoms in each assigned molecular formulas.

Detected ions not observed as a homologous series (compounds with the same DBE but varying carbon number) of at least five members and classes with a relative abundance (ra %) below 0.15% were excluded from the analysis. More than 20 000 molecular formulas for WA, RA, and IAA were assigned. The assigned formulas were compared in terms of their relative abundance, which is expressed as a percentage of the identified heteroatom classes.

Isolation of precursor ions within a 4 Da range at m/z 450 and 650 were selected for fragmentation via a mass-filter quadrupole, followed by multi-notch stored waveform inverse Fourier transform (SWIFT) using a method previously described.[5,32−34] The multi-notch SWIFT process helps to isolate ions with a mass defect <0.25000 Da (DBE > 15−18), which remain in the ICR for subsequent fragmentation at a remarkably low pressure (<1 × 10^{−10} Torr). The precursor ions were subjected to infrared radiation (λ = 10.6 μm, 40 W irradiation, Synrad CO_2 laser, Mukilteo, WA) for 50−2000 ms. The produced fragments were analyzed by conventional FT-ICR MS. The boundary between single-core and multi-core structures was determined as the difference between the abundance-weighted (AW) average DBE value of the precursor ions and their AW standard deviation. The boundary is identified by the red dashed lines in the IRMPD data.

■ RESULTS AND DISCUSSION

WA, RA, and IAA Fractions. Compositional similarity between WA and RA fractions was observed. This is not surprising since WA is composed of ~98.5 wt % of RA. Therefore, detailed comparisons of WA to RA and IAA are not presented; however, for reference, the WA data are provided in the Supporting Information (iso-abundance-contoured plots of DBE vs carbon number for different heteroatom classes, Figures S1−S7).

Figure 1 compares the relative abundance (%) of different heteroatom classes (elemental composition assigned from mass spectral peaks) in RA and IAA. WA is also included to highlight the similarity between WA and RA fractions. Heteroatom classes were assigned on the basis of the elemental compositions, for example, species containing one nitrogen atom were assigned to the N_1 class and species containing no heteroatoms were assigned to the HC class. It is clear that the heteroatom content differentiates the E-SARA fractions, with ~53% of IAA containing two or more heteroatoms, compared with just
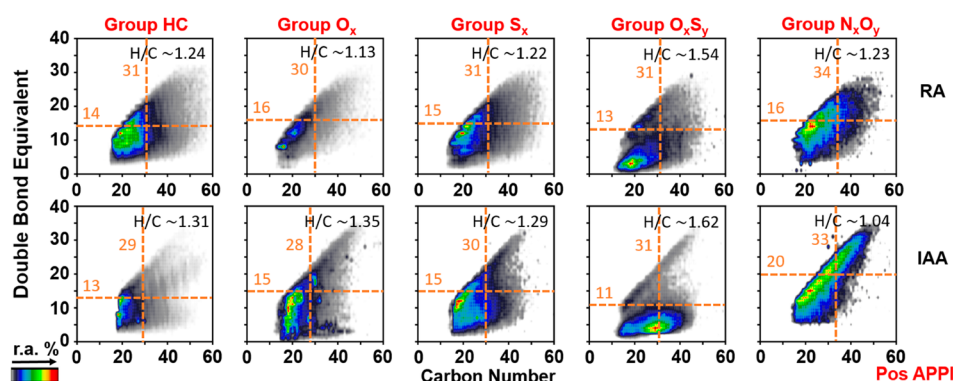
Figure 2. Iso-abundance-contoured plots of DBE vs carbon number for different heteroatom groups of RA (top row) and IAA (bottom row). The relative abundance (%) is shown by the color key with gray and red representing low and high relative abundances, respectively. Dashed lines represent the AW average DBE and carbon number. The AW average H/C mass ratio is shown as the inset.

~30% for RA (Figure 1). The molecular weight distributions for all three samples are shown for the m/z range 200−850.

The WA and RA samples revealed similar molecular weight distributions, which spanned from 200 to ~650 Da, and a peak intensity in the region of 300 Da (average molecular weights of 440 and 441 Da, respectively). For IAA, a clear bimodal distribution was observed, with the two peak intensities measured in the region of 250 and 550 Da and the molecular weight distribution measured up to ~750 Da (average molecular weight of 447 Da). Similar molecular weight distributions for RA and IAA were previously found when measured using nanostructure-assisted laser desorption mass spectroscopy (NALDI-MS),[23] although the values reported by NALDI-MS were slightly higher. The smaller molecular weight values reported by APPI FT-ICR MS results from using APPI, which produces ions with a higher internal energy, reducing the possibility of detecting low-order aggregates (dimers, trimers, etc.). Larger aggregates are not observed in the mass spectra because the ICR cell is tuned for detecting compounds with m/z between 100 and 1500. The bimodal molecular weight distribution of IAA may hint at the mechanism for interfacial film formation and growth, with a bimodal distribution possibly supporting a two-step adsorption process. While this is currently speculative, it suggests that more characterization of the smaller and larger IAA fractions could provide further insights, although this is currently beyond the scope of the current study.

Compound classes can be sorted into heteroatom groups. For instance, the classes S1, S2, S3, etc., belong to the group S_x. Comparison of the relative abundance of each heteroatom group for IAA and RA (Figure S8) indicated that the HC, N_x, S_x, and N_xS_y groups were depleted in the IAA fraction. Moreover, IAA was found to be enriched in O_x groups, particularly, compounds with a high content of oxygen atoms, such as O_{3-5}, N_1O_{2-3} (N_xO_y), and $O_{2-4}S_{1-3}$ (O_xS_y) heteroatom classes. These findings agree with those of the previous studies of Czarnecki and co-workers who confirmed enrichment of O_x and O_xS_y groups in the interfacial material that stabilizes water-in-crude oil emulsions.[15−17] The enrichment of O_x and O_xS_y groups is also consistent with the results of bulk elemental composition analysis of IAA and RA fractions: S and O contents of IAA (heavy crude oil) were found to be 4.43 wt % (S) and 4.57 wt % (O), compared with 3.45 wt % (S) and 2.41 wt % (O) for RA.[23]

The relative abundance of vanadyl porphyrins ($N_4O_1V_1$) in both RA and IAA fractions was found to be small, with less $N_4O_1V_1$ being measured in the IAA fraction. While recent

studies have highlighted the importance of porphyrins in stabilizing emulsions,[46] it is worth noting that the lack of detection of vanadyl porphyrins in MS may be due to the strong aggregation tendency of the IAA fraction,[47,48] which decreases its monomer ion yield in APPI and precludes detection of certain compound classes. Vanadyl porphyrins that were detected in all samples revealed similar ranges of carbon number (~26−36) and DBE (~18−22). The molecular composition (DBE vs carbon number plots) is shown in the Supporting Information, Figure S7.

Heteroatom groups can be further analyzed by the iso-abundance-contoured plots of DBE vs carbon number. Figure 2 presents the DBE vs carbon number plots of HC, O_x, S_x, O_xS_y, and N_xO_y groups for RA and IAA.
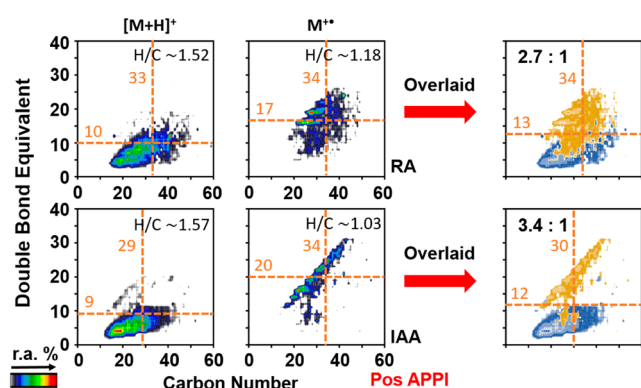
The iso-abundance-contoured plots (Figure 2) confirmed different molecular compositions of RA and IAA. Except for the N_xO_y group, which accounts for ~5% of the heteroatom-containing compounds in RA and IAA, all other heteroatom groups exhibited a higher H/C mass ratio in IAA than in RA. The AW average H/C mass ratios for the RA and IAA fractions were 1.25 and 1.39. Using the same extraction procedure and the same batch of heavy crude oil, slightly lower H/C mass ratios were measured by elemental analysis (RA = 1.04 and IAA = 1.21).[23] Although other studies have found APPI to underestimate asphaltene H/C ratios compared to elemental analysis,[49] it is likely that the discrepancy in the current study results from the sample consisting of lower DBE, oxygen-rich ions, which are more prone to gas phase/proton transfer reactions during dopant-assisted APPI, resulting in efficient ionization of compounds with high proton affinities.[34,50−52] Conversely, highly aromatic and oxygen deficient samples are more prone to ionize as radical cations, which would result in lower MS-derived H/C ratios. In our case, there were higher MS-derived H/C ratios than bulk elemental analysis. Regardless, the trend observed by MS was consistent with bulk elemental analysis; the IAA fraction is less aromatic than RA. Apart from the N_xO_y group, the average carbon number and AW average DBE of the heteroatom groups in IAA were either equivalent or lower than in RA.

The AW average DBE values for N_xO_y in RA and IAA were 16 and 20, with less than 1% of the detected ions having a DBE > 30 (highly aromatic species) for RA and 3.6% for IAA. A Pearson correlation analysis between DBE and carbon number for the N_xO_y group revealed correlation coefficients of 0.52 and 0.72 for RA and IAA, respectively. A narrower distribution (DBE vs

carbon number) and high DBE values for IAA suggests that the N-containing species are most likely associated with large polyaromatic cores.

Heteroatomic functionalities of the O_xS_y group in IAA are less likely to be contained within aromatic cores, especially in species containing multiple oxygen atoms such as O_3S_3 and O_4S_3, which feature remarkably low DBE values (Figure S5). For RA, only heteroatom classes up to O_2S_2 (Figure S2) were detected at levels above the measurement threshold (abundance $>6\sigma$), whereas for IAA, the O_xS_y group included species up to O_4S_3 (Figure S5). Further analysis of the O_x and O_xS_y groups showed a decrease in the AW average DBE with increasing O content. For example, for the O_x group, the AW average DBE for RA and IAA decreased from 16 (O_1) to 12 (O_3) and 15 (O_1) to 9 (O_5), respectively. Similar changes in the AW average DBE of O_xS_y group for RA and IAA were also observed (Figures S2, S3 and S5, Supporting Information). A reduction in the AW average DBE for higher-order oxygen containing groups is consistent with the results from previous studies where higher-order oxygen containing groups were associated with lower aromaticity asphaltene structures.[34,53−55]

The APPI ion source produces protonated molecules ([M + H]$^+$) and radical cations (M$^{+\bullet}$),[50] with separate iso-abundance-contoured plots of DBE vs carbon number revealing differences in their compositional range. In Figure 2, it was shown that the O_xS_y group of IAA had a high abundance of species below the AW average DBE of 11. Comparing the protonated compounds ([M + H]$^+$) and radical cations (M$^{+\bullet}$) for the heteroatom class O_1S_2 (chosen due to its high relative abundance), Figure 3

Figure 3. Iso-abundance-contoured plots of DBE vs carbon number of O_1S_2 protonated ([M + H]$^+$) and radical (M$^{+\bullet}$) cations for RA (top row) and IAA (bottom row). Dashed lines represent AW average DBE and carbon number. The AW average H/C mass ratio is shown inset. Overlaid iso-abundance-contoured plots with protonated and radical species being highlighted by the blue-shaded and yellow-shaded regions, respectively. The protonated-to-radical ratio is shown in each corresponding plot.

shows that the protonated species (O_1S_2 [M + H]$^+$) have an AW average DBE $\leq$ 10 and feature a compositional range at lower DBE than the radical cations. A better separation of protonated and radical cation species was seen for the IAA fraction, as is clearly shown by the overlaid iso-abundance-contoured plots in Figure 3, as well as being confirmed by the greater difference in AW average DBE values: IAA = 11 and RA = 7. Moreover, the abundance ratio of protonated-to-radical cations ([M + H]$^+$/M$^{+\bullet}$) was greater in IAA than in RA (IAA = 3.4 and RA = 2.7), demonstrating that IAA compounds preferentially ionize via protonation, which correlates with a higher tendency to

hydrogen-bond in solution. Furthermore, the protonated species of both RA and IAA reveal a higher H/C mass ratio (RA ~ 1.52; IAA ~ 1.57) than the radical cations (RA ~ 1.18; IAA ~ 1.03). In summary, the IAA fraction is enriched in low aromatic molecular structures, which have a tendency to form hydrogen bonds.

The relative abundance of the O_xS_y group in RA and IAA is 11.7% and 25.4%, representing a significant difference between the two asphaltene fractions (the relative abundances of HC, O_x, S_x, N_x, O_xS_y, N_xO_y, $N_xO_yS_z$, and $N_xO_yV_z$ groups are shown in Figure S8). Given this difference and the fact that IAA contains higher amounts of S and O, with a likely significant enrichment in the S=O functional group,[21−25] it can be postulated that the water-in-oil stabilizing asphaltenes are predominantly composed of low aromaticity molecular structures containing O_xS_y groups that readily ionize as protonated molecules. These "atypical" structures are classified as asphaltenes as a result of their functionality and polarity rather than high aromaticity.

Fragmentation of IAA and RA. In an attempt to determine the predominant structure (single-core or multi-core) of IAA and RA, precursor ions of relatively high molecular weight (m/z 650), where multi-core structures are likely to be observed (if they are present),[56−58] were isolated via mass-resolving quadrupole and SWIFT multi-notch and fragmented by IRMPD (see Figure 4 for the fragmentation spectra). Fragmentation data of lower molecular weight (m/z 450) ions are shown in the Supporting Information to highlight the sensitivity of the single-core/multi-core predominance on molecular weight. IRMPD yields the most stable species by removing alkyl-chains and cleaving the alkyl bridges between aromatic cores, leaving stable aromatic cores unfragmented.[32,59] Greater fragmentation of IAA was verified by considering the abundance of species below and above a threshold of m/z 400. This threshold was chosen as alkyl-substituted low ring number polycyclic aromatic hydrocarbons (PAHs), such as naphthalene, phenanthrene, pyrene, and dibenzothiophene, have masses below m/z 400. The abundance ratio of species below m/z 400 was 1.45 and 2.13 for RA and IAA, confirming greater fragmentation of IAA. While this supports the view that IAA contains smaller cores (lower M_w), which are aryl-linked or linked by alkyl-chains, the increased fragmentation of IAA may also result from the higher oxygen content, with carboxylic acid, ketone, and sulfoxide functional groups known to absorb infrared light more efficiently.[34]

In fragmentation, single-core structures follow a dealkylation pattern, whereby only the carbon number decreases, whereas multi-core structures lose both the carbon number and DBE. The fragmentation patterns for both RA and IAA show a reduction in DBE and carbon number, signifying the presence of multi-core structures in each fraction. Dealkylation is more evident for RA at DBE 25 and 30, suggesting a greater fraction of single-core motifs. Fragmentation of IAA led to abundant low DBE (10) and low carbon number (16) fragment ions, whereas RA revealed fragments with intermediate DBE (30) and carbon numbers (44). These intermediates likely result from deal-kylation of large aromatic structures (single-core) and fragmentation of multi-core structures. To reflect the abundance of single-core and multi-core motifs in IAA and RA, we define a boundary between these two structures (identified by the red line in Figure 5). The boundary is determined by subtracting the AW standard deviation from the AW average DBE value for the assigned precursor ions,[32] with the boundary at DBE of 20 and 18 for RA and IAA. The fragment ions with DBE values below
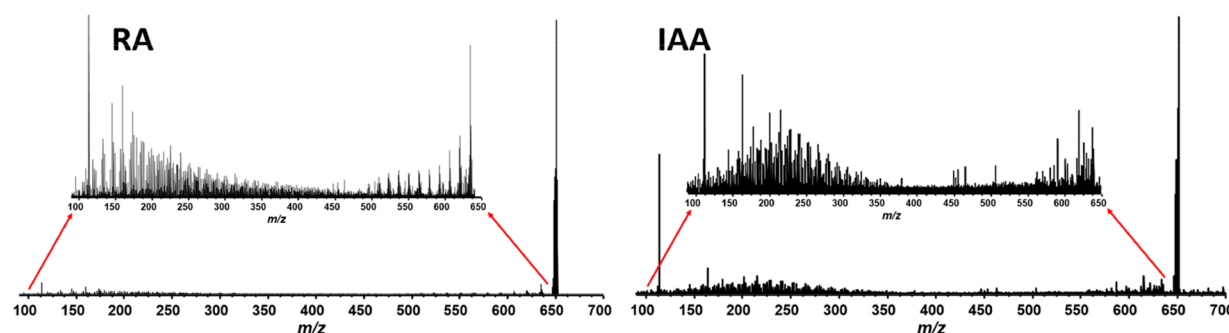
Figure 4. Mass spectra of the isolated precursor ions (m/z 650) (below spectra) and fragment ions detected following irradiation of the precursor ions (above spectra) by IRMPD for RA (left) and IAA (right).
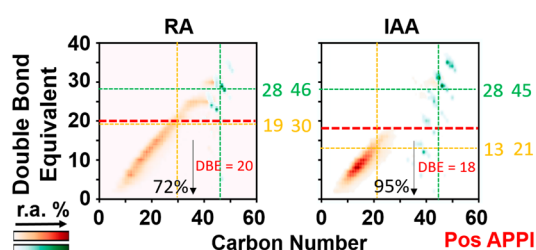
Figure 5. Combined iso-abundance-contoured plots of DBE vs carbon number of the precursor and fragment ions from RA (left) and IAA (right). The precursor and fragmented ions are identified by the green and orange color maps, respectively. Green and orange lines represent the AW average DBE (first number) and carbon number (second number) for the precursor and fragment ions. The red line represents the boundary to identify between single-core (above) and multi-core (below) structures, with the percentage value (inset) confirming the abundance of fragment ions representing multi-core motifs.

the boundary are likely produced from fragmenting multi-core structures, while those fragment ions with DBE values above the boundary are likely produced from fragmenting single-core motifs. The abundance of fragment ions below the boundary was 72% for RA and 95% for IAA, confirming that the high DBE precursor ions of IAA with m/z 650 are almost entirely multi-core structures, whereas the RA fraction is a mixture of single-core and multi-core motifs. A greater abundance of multi-core motifs in IAA likely supports our recent SANS data, which showed that the IAA fraction form larger and more porous nanoaggregates compared to the RA fraction.[23] It was speculated that the larger nanoaggregates were formed due to the presence of more functional groups (carbonyl and sulfoxide), which can now be further understood by the differences in the molecular structure of the two asphaltene subfractions. These findings agree with a molecular mechanics study,[60] which showed multi-core asphaltenes form more complex (bridged and tangled) aggregates.

It is possible to discern "typical" structures of RA and IAA fractions from the changes in the AW average DBE values and carbon numbers. For RA and IAA, the AW average DBE values decreased from 46 to 30 (RA) and 45 to 21 (IAA) and the carbon numbers decreased from 28 to 19 (RA) and 28 to 13 (IAA). Such fragmentation represents a reduction in the molecular weight by ~34% and ~53% for RA and IAA. For complex mixtures, the reduction in molecular weight can occur through a number of different fragmentation pathways: (i) dealkylation; (ii) splitting of two equally sized aromatic cores; (iii) splitting of two aromatic cores of different size; and (iv)

splitting of multiple aromatic cores. On the basis of the changes in molecular weight and the abundance of fragment ions, we postulate that RA is composed of a mixture of single-core and multi-core motifs, while IAA is predominantly multi-core structures. Figures S13 and S14 show the mass spectra and iso-abundance-contoured plots of DBE vs carbon number for the fragmented ions of RA and IAA from precursor ions of m/z 450. The fragmentation patterns were found to be similar with most of the fragmented ions generated from single-core motifs (RA = 62%, IAA = 73%). A greater abundance of single-core structures for the lower molecular weight species supports the theory that a carbon limit exists for asphaltenes, where the further addition of carbon leads to the formation of multi-core structures, as peri-condensation becomes less favored/likely.[61]

With a higher abundance of O_xS_y in IAA than RA, fragmentation of the O_xS_y precursor ions (m/z 650) was compared (see Figure S15). The RA fraction showed significant dealkylation, with only 39% of the fragment ions determined to be multi-core motifs. Fragmentation of the IAA precursor ion led to a greater reduction in the AW average DBE and carbon number, with 62% of the fragment ions resulting from multi-core structures.

To estimate the likely location of heteroatoms in RA and IAA, N/C, O/C, and S/C ratios before and after IRMPD fragmentation were compared and summarized in Table 1. We

Table 1. Comparison of Heteroatom (N, O, and S) to Carbon Ratio of m/z 650 Ions before and after Fragmentation by IRMPD

sample	N/C	O/C	S/C
precursor RA	0.0126	0.0177	0.0166
fragment RA	0.0163	0.0141	0.0189
% change	*29.7*	*−20.2*	*14.2*
precursor IAA	0.0152	0.0367	0.0253
fragment IAA	0.0131	0.0156	0.0207
% change	*−13.9*	*−57.5*	*−17.9*

assume that strongly negative values are associated with a reduction in heteroatom content as a result of the heteroatoms being located in aliphatic side chains and thus not detected following IRMPD, because the charge most likely remains in the aromatic cores. Strongly positive values are associated with heteroatoms more likely to be found in aromatic cores, as carbon is lost in the aliphatic side chains but the heteroatom content is retained. The data shows that in both RA and IAA, N is most likely found within aromatic cores and O is most likely located in aliphatic chains. This supports our earlier finding that N-
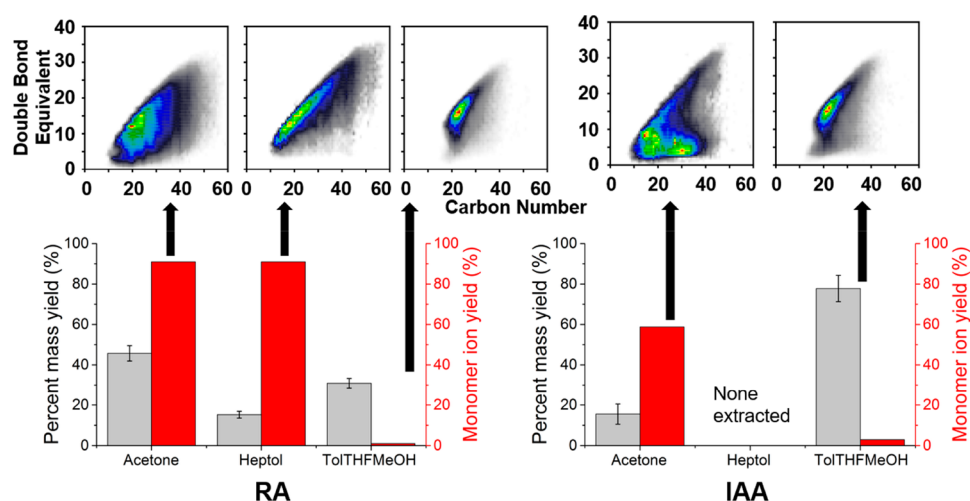
Figure 6. Mass yield (%; gray bar) and monomer ion yield (%; red bar) for RA (left) and IAA (right) fractions separated by the extrography method. The iso-abundance-contoured plots of DBE vs carbon number for each sample are provided above.

**Table 2. Summary of Parameters Used for Model Structure Determination of RA and IAA**[a]

	RA				
	HC	N_x	O_x	O_xS_y	S_x
abundance in fraction	32%	11%	13%	12%	23%
C# and DBE	24 and 10	23 and 12	21 and 12	19 and 3	22 and 12
reduction in C# and DBE by IRMPD	75% and 82%	n/a	8% and 12%	9% and 14%	69% and 64%
functional groups	none	pyridine[64]	carbonyl[18] carboxylic acid[65]	carbonyl[18] carboxylic acid[65] thiophene[26,27,66] sulfoxide[26,27,66] sulfone[26,27,66]	thiophene[26,27,66] sulfide[26,27,66] sulfone[26,27,66]
heteroatom content	● ~30% of fraction contains no heteroatoms ● >35% of fraction contains only 1 heteroatom (S1, N1, or O1)				
	IAA				
	HC	N_xO_y	O_x	O_xS_y	S_x
abundance in fraction	22%	8%	27%	25%	11%
C# and DBE	19 and 8	26 and 13	18 and 12	29 and 4	20 and 12
reduction in C# and DBE by IRMPD	73% and 79%	10% and 14%	74% and 71%	64% and 40%	71% and 71%
functional groups	none	pyridine[64]	carbonyl[18] carboxylic acid[65]	carbonyl[18] carboxylic acid[65] thiophene[26,27,66] sulfoxide[26,27,66] sulfone[26,27,66]	thiophene[26,27,66] sulfide[26,27,66] sulfone[26,27,66]
heteroatom content	● ~50% of fraction contains polyheteroatomic species ● oxygen-containing species noticeably abundant				

[a]The reduction in carbon number (C#) and DBE was taken as the difference between modal values for the precursor and fragmented ions, with n/a reported for heteroatom groups where precursor ions were not detected.

containing species have a high DBE and therefore are highly aromatic (see Figures S1, S6, and S7).

Fractionation by Extrography. Further fractionation of RA and IAA was made using the extrography method to yield asphaltene fractions enriched in single-core and multi-core structures. By using acetone, Heptol 1:1, and Tol/THF/MeOH as extracting solvents, it is possible to selectively extract highly aromatic compounds, nonpolar species, and polar molecules interacting via hydrogen bonding with the silica gel.[5,32] Figure 6 shows the mass yield (%) and the monomer ion yield (%; MIY) for both RA and IAA eluted using the three solvents, with the mass yield reflecting the solubility and the MIY the ionization efficiency of each fraction.

Through comparing the mass yields of the extrography fractions, the data supports our earlier finding and confirms that RA is a mixture of abundant single-core and multi-core structures, while IAA is enriched in multi-core motifs. Acetone elution led to mass yields of 45.7 ± 3.8% and 15.5 ± 5.0% for RA and IAA, respectively. The higher monomer ion yield of RA (acetone eluted) compared to IAA is in good agreement with the ion production efficiency of single-core and multi-core structures,[5,32−34,56] with the low monomer ion yield of IAA resulting from a predominance of highly aggregated multi-core species during APPI ionization. While extrography has previously been used to separate highly aromatic compounds and polar molecules, the prior fractionation of WA by the E-
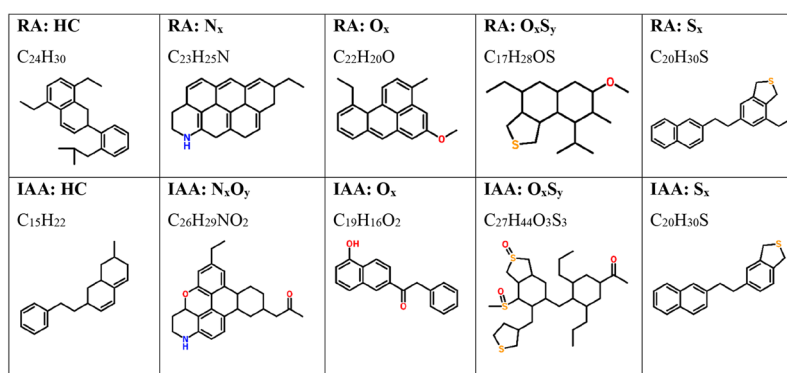
Figure 7. Proposed structures of RA (above) and IAA (below) fractions. These structures were optimized on the basis of the data given in Table 2.

SARA method led to an abundance of polar species (O_xS_y) being eluted with acetone. The high relative abundance of O_xS_y in IAA (acetone eluted) may result from a strong interaction between the O_xS_y heteroatom group and the double bonded oxygen in acetone. Figure S11 confirms that the O_xS_y heteroatom group of IAA extracted by acetone is of low aromaticity (AW average DBE = 9).

A second elution with Heptol 1:1 led to poor extraction of both RA and IAA, with the mass yield for RA equal to 15.2 ± 1.7% and negligible mass recovered for IAA, suggesting that both fractions, in particular IAA, are enriched with polar compounds. The high AW average DBE of RA extracted by Heptol 1:1 (Figure 6) confirms that the nonpolar species are highly aromatic. Moreover, a third elution with Tol/THF/MeOH 2:2:1 led to a significant extraction of IAA (77.8 ± 6.5%), confirming the high polarity of the multi-core structures in IAA. A very high abundance of protonated O_xS_y species was found in IAA (Figure 3), with these highly polar species exhibiting lower DBE values than those of the radical ions. Further analysis of the extrography fractions by heteroatom groups is provided in Figures S12−S15.

Model Structures. Using the (+) APPI FT-ICR MS analysis, previous characterization data of RA and IAA,[21,23,25] and other reported asphaltene characterization data, model structures for RA and IAA motifs are proposed. This is a similar approach to the development of the surrogate model structures proposed by Jameel et al.,[62] following extensive characterization of heavy fuel oils.[63] However, rather than determining a "typical" structure for RA and IAA using only the abundance weighted average values (M_w, carbon number, DBE), where differences were found to be negligible, five model structures for each asphaltene fraction were developed to highlight the apparent differences between the two fractions. Table 2 summarizes the parameters used to construct the model asphaltene motifs, emphasizing the abundant heteroatom groups, modal values of carbon numbers and DBEs, and size reduction by IRMPD as calculated using modal values of carbon number and DBE. The relative abundance of the heteroatom groups should be used in model structure simulations to scale the heteroatom contents to correspond to bulk fraction measurements. With scaling applied to the model structures, the H/C, N/C, O/C, and S/C ratios of RA are 1.20, 0.005, 0.01, and 0.02, respectively, compared to 1.16, 0.003, 0.06, and 0.04 for IAA. This compares to ratios of 1.04, 0.02, 0.06, and 0.02 (RA) and 1.21, 0.03, 0.09, and 0.04 (IAA) from bulk elemental analysis,[23] which means that the heteroatom content is slightly underestimated in the proposed model structures after scaling by the relative abundance as determined by FT-ICR MS.

The fragmentation data (m/z 650, Figure 5) confirmed IAA to be predominantly multi-core, while RA is a mixture of single-core and multi-core motifs. For the HC class (Figure 7), the large reduction in both carbon number and DBE (by IRMPD) for both RA and IAA indicated a predominance of multi-core structures, with the molecular size taken from the modal value of carbon number. It should be noted that the predominance of multi-core structures is likely over exaggerated as fragments containing no heteroatoms readily cleave from heteroatom-containing groups. The H/C mass ratios, carbon number, and DBE as well as heteroatom content of the proposed molecular structures in Figure 7 correspond to the FT-ICR MS data in Figures 1 and 2 and Table 2 (a consistent approach for structure determination was followed for all heteroatom groups).

The O_xS_y groups were found to be abundant in IAA, principally the O_3S_3 heteroatom class (Figure 1), with these heteroatom groups mostly associated with multi-core motifs (Figure S15). For IAA, the O-containing species (O_x, O_xS_y, and N_xO_y) accounted for 60% of the fraction by abundance (Figure S8), while their presence in RA was substantially lower (30%) and mostly associated with single-core motifs. The remarkably low DBE values for O_x and O_xS_y groups in IAA (Figure 2) suggests the heteroatoms to be located in alkyl-chains rather than the aromatic cores. This has been previously suggested as likely or even typical, such as the presence of phenolic groups.[67,68] Ren et al.[31] confirmed the O_1S_1 class species to be sulfoxides, but an abundance of higher-order O_xS_y-containing species indicates the likely presence other sulfur-containing species such as sulfone.[26,27,66] On the basis of previous findings, the O_x groups are most likely to be carbonyl functional groups.[25]

For the S_x group, the DBEs and carbon numbers for RA and IAA were almost equivalent and showed a similar high degree of fragmentation, indicating a prevalence of multi-core structures. While the relative abundance of S_x was found to be greater in RA than IAA, this is likely attributed to the greater association of S and O in IAA (abundance of O_xS_y groups). From Figure 1, it is likely that S_x exits as one heteroatom, which is most probably thiophene and sulfide.[25,26,66]

For the N-containing species the relative abundance of N_x and N_xO_y heteroatom groups were 11% and 5% for RA and 5% and 8% for IAA. Table 2 shows a small reduction in the carbon number and DBE of the N_xO_y group (IAA) following fragmentation, confirming its association to a large, single aromatic core with few (small) aliphatic side chains. As no N_x

precursor ions were detected for RA, it was not possible to ascertain the degree of fragmentation.

It should be emphasized that these model structures for RA and IAA have been proposed to reflect key differences between the two fractions and are not intended to diminish the complexity of characterizing asphaltenes. Its purpose is to provide new insights regarding the molecular structure and chemistry based on abundant properties, which likely govern both bulk and interfacial behaviors of asphaltenes.

CONCLUSIONS

This study follows a methodology reported in a series of papers characterizing the physicochemical properties of interfacially active asphaltenes (IAA) and remaining asphaltenes (RA) that are extracted using the E-SARA method. Earlier studies have revealed differences in elemental composition, M_w, and nanoaggregate size and shape, yet differences in the molecular structure and chemistry of these two asphaltene fractions remained to be explored. Asphaltenes were extracted from a South American heavy crude oil and further separated into RA and IAA by the E-SARA method, with IAA accounting for ~1.5 wt % of the whole asphaltene fraction. Using positive-ion atmospheric pressure photoionization 9.4 T Fourier transform ion cyclotron resonance mass spectroscopy ((+)APPI 9.4 T FT-ICR MS) and infrared multiphoton dissociation (IRMPD), the discriminating properties between the two asphaltene fractions are

(1) IAA is enriched in O_x and O_xS_y groups with an abundance of higher-order oxygen-containing species. RA is enriched in single heteroatom classes, O_1, S_1, and N_1.

(2) For all heteroatom groups except N_xO_y, the H/C mass ratio of IAA was higher than that of RA, confirming the less aromatic nature of IAA.

(3) Fragmentation of precursor ions (m/z 650) of RA and IAA revealed a mixture of single-core and multi-core motifs in RA and an abundance of multi-core structures in IAA.

(4) IAA compounds preferentially ionize via protonation, which correlates with a higher tendency to hydrogen-bond in solution.

(5) N- and O-containing species are most likely found within aromatic cores and aliphatic side chains, respectively.

(6) The molecular structure of IAA is "atypical" for asphaltenes as a result of their functionality and polarity rather than high aromaticity.

Critically, this study revealed that the asphaltene fraction most likely responsible for emulsion stabilization and fouling problems does not entirely conform to the molecular description of an asphaltene. This new insight into the molecular structure and chemistry of IAA will help design appropriate chemistries to mitigate asphaltene-related problems, the success of which is strongly dependent on the cooperative interaction between the additives and asphaltene molecules/nanoaggregates.

ASSOCIATED CONTENT

ⓢ Supporting Information

The Supporting Information is available free of charge at https://pubs.acs.org/doi/10.1021/acs.energyfuels.0c02752.

Figures of iso-abundance plots, relative abundances of the heteroatom groups, and mass spectra (PDF)

AUTHOR INFORMATION

Corresponding Author

David Harbottle − *School of Chemical and Process Engineering, University of Leeds, Leeds LS2 9JT, United Kingdom;* ⓞ orcid.org/0000-0002-0169-517X; Phone: +44(0)113 343 4154; Email: d.harbottle@leeds.ac.uk

Authors

Dewi A. Ballard − *School of Chemical and Process Engineering, University of Leeds, Leeds LS2 9JT, United Kingdom;* ⓞ orcid.org/0000-0002-5506-199X

Martha L. Chacón-Patiño − *National High Magnetic Field Laboratory, Florida State University, Tallahassee, Florida 32306, United States;* ⓞ orcid.org/0000-0002-7273-5343

Peiqi Qiao − *Department of Chemical and Materials Engineering, University of Alberta, Edmonton AB T6G 2R3, Canada*

Kevin J. Roberts − *School of Chemical and Process Engineering, University of Leeds, Leeds LS2 9JT, United Kingdom;* ⓞ orcid.org/0000-0002-1070-7435

Robert Rae − *Infineum UK Ltd., Abingdon, Oxfordshire OX13 6BB, United Kingdom*

Peter J. Dowding − *Infineum UK Ltd., Abingdon, Oxfordshire OX13 6BB, United Kingdom*

Zhenghe Xu − *Department of Chemical and Materials Engineering, University of Alberta, Edmonton AB T6G 2R3, Canada; Department of Materials Science and Engineering, Southern University of Science and Technology, Shenzhen 518055, China;* ⓞ orcid.org/0000-0001-8118-1920

Complete contact information is available at:
https://pubs.acs.org/10.1021/acs.energyfuels.0c02752

Notes

ABBREVIATIONS

APPI, atmospheric pressure photoionization; AW, abundance weighted; E-SARA, extended-SARA; FT-ICR MS, Fourier transform ion cyclotron resonance mass spectrometry; IAA, interfacially active asphaltenes; IRMPD, infrared multi-photon dissociation; NALDI-MS, nanostructure-assisted laser desorption mass spectroscopy; RA, remaining asphaltenes; SWIFT, stored waveform inverse Fourier transform; WA, whole asphaltenes

■ REFERENCES

(1) McKenna, A. M.; Chacón-Patiño, M. L.; Weisbrod, C. R.; Blakney, G. T.; Rodgers, R. P. Molecular-Level Characterization of Asphaltenes Isolated from Distillation Cuts. *Energy Fuels* **2019**, *33* (3), 2018−2029.

(2) Gray, M. R.; Tykwinski, R. R.; Stryker, J. M.; Tan, X. Supramolecular Assembly Model for Aggregation of Petroleum Asphaltenes. *Energy Fuels* **2011**, *25* (7), 3125−3134.

(3) Mullins, O. C. The Asphaltenes. *Annu. Rev. Anal. Chem.* **2011**, *4* (1), 393−418.

(4) Schuler, B.; Zhang, Y.; Liu, F.; Pomerantz, A. E.; Andrews, A. B.; Gross, L.; Pauchard, V.; Banerjee, S.; Mullins, O. C. Overview of Asphaltene Nanostructures and Thermodynamic Applications. *Energy Fuels*, in press, **2020**.

(5) Chacón-Patiño, M. L.; Rowland, S. M.; Rodgers, R. P. Advances in Asphaltene Petroleomics. Part 1: Asphaltenes Are Composed of Abundant Island and Archipelago Structural Motifs. *Energy Fuels* **2017**, *31* (12), 13509−13518.

(6) Qiao, P.; Harbottle, D.; Tchoukov, P.; Masliyah, J.; Sjoblom, J.; Liu, Q.; Xu, Z. Fractionation of Asphaltenes in Understanding Their Role in Petroleum Emulsion Stability and Fouling. *Energy Fuels* **2017**, *31* (4), 3330−3337.

(7) Mullins, O.; Sheu, E.; Hammami, A.; Marshall, A. *Asphaltenes, Heavy Oils, and Petroleomics*; Springer New York: New York, NY, 2007.

(8) Spiecker, P. M.; Gawrys, K. L.; Kilpatrick, P. K. Aggregation and solubility behavior of asphaltenes and their subfractions. *J. Colloid Interface Sci.* **2003**, *267* (1), 178−93.

(9) Wattana, P.; Fogler, H. S.; Yen, A.; Carmen Garcìa, M. D.; Carbognani, L. Characterization of Polarity-Based Asphaltene Subfractions. *Energy Fuels* **2005**, *19* (1), 101−110.

(10) Pinto, F. E.; Barros, E. V.; Tose, L. V.; Souza, L. M.; Terra, L. A.; Poppi, R. J.; Vaz, B. G.; Vasconcelos, G.; Subramanian, S.; Simon, S.; Sjöblom, J.; Romão, W. Fractionation of asphaltenes in n-hexane and on adsorption onto CaCO3 and characterization by ESI(+)FT-ICR MS: Part I. *Fuel* **2017**, *210*, 790−802.

(11) Kilpatrick, P. K. Water-in-Crude Oil Emulsion Stabilization: Review and Unanswered Questions. *Energy Fuels* **2012**, *26* (7), 4017−4026.

(12) Spiecker, P. M.; Kilpatrick, P. K. Interfacial Rheology of Petroleum Asphaltenes at the Oil-Water Interface. *Langmuir* **2004**, *20* (10), 4022−4032.

(13) Verruto, V. J.; Le, R. K.; Kilpatrick, P. K. Adsorption and Molecular Rearrangement of Amphoteric Species at Oil-Water Interfaces. *J. Phys. Chem. B* **2009**, *113* (42), 13788−13799.

(14) Wu, X. Investigating the Stability Mechanism of Water-in-Diluted Bitumen Emulsions through Isolation and Characterization of the Stabilizing Materials at the Interface. *Energy Fuels* **2003**, *17* (1), 179−190.

(15) Stanford, L. A.; Rodgers, R. P.; Marshall, A. G.; Czarnecki, J.; Wu, X. A.; Taylor, S. Detailed Elemental Compositions of Emulsion Interfacial Material versus Parent Oil for Nine Geographically Distinct Light, Medium, and Heavy Crude Oils, Detected by Negative- and Positive-Ion Electrospray Ionization Fourier Transform Ion Cyclotron Resonance Mass Spectrometry. *Energy Fuels* **2007**, *21* (2), 973−981.

(16) Stanford, L. A.; Rodgers, R. P.; Marshall, A. G.; Czarnecki, J.; Wu, X. A. Compositional Characterization of Bitumen/Water Emulsion Films by Negative- and Positive-Ion Electrospray Ionization and Field Desorption/Ionization Fourier Transform Ion Cyclotron Resonance Mass Spectrometry. *Energy Fuels* **2007**, *21* (2), 963−972.

(17) Czarnecki, J. Stabilization of Water in Crude Oil Emulsions. Part 2. *Energy Fuels* **2009**, *23* (3), 1253−1257.

(18) Subramanian, S.; Simon, S.; Gao, B.; Sjöblom, J. Asphaltene fractionation based on adsorption onto calcium carbonate: Part 1. Characterization of sub-fractions and QCM-D measurements. *Colloids Surf., A* **2016**, *495* (Supplement C), 136−148.

(19) Subramanian, S.; Sørland, G. H.; Simon, S.; Xu, Z.; Sjöblom, J. Asphaltene fractionation based on adsorption onto calcium carbonate: Part 2. Self-association and aggregation properties. *Colloids Surf., A* **2017**, *514*, 79−90.

(20) Rogel, E.; Ovalles, C.; Moir, M. Asphaltene Chemical Characterization as a Function of Solubility: Effects on Stability and Aggregation. *Energy Fuels* **2012**, *26* (5), 2655−2662.

(21) Yang, F.; Tchoukov, P.; Dettman, H.; Teklebrhan, R. B.; Liu, L.; Dabros, T.; Czarnecki, J.; Masliyah, J.; Xu, Z. Asphaltene Subfractions Responsible for Stabilizing Water-in-Crude Oil Emulsions. Part 2: Molecular Representations and Molecular Dynamics Simulations. *Energy Fuels* **2015**, *29* (8), 4783−4794.

(22) Yang, F.; Tchoukov, P.; Pensini, E.; Dabros, T.; Czarnecki, J.; Masliyah, J.; Xu, Z. Asphaltene Subfractions Responsible for Stabilizing Water-in-Crude Oil Emulsions. Part 1: Interfacial Behaviors. *Energy Fuels* **2014**, *28* (11), 6897−6904.

(23) Ballard, D. A.; Qiao, P.; Cattoz, B.; Dowding, P. J.; Prevost, S.; Alshamsi, M.; Charpentier, T.; Roberts, K. J.; Xu, Z.; Harbottle, D. Aggregation Behavior of E-SARA Asphaltene Fractions Studied by Small-Angle Neutron Scattering. *Energy Fuels* **2020**, *34* (6), 6894−6903.

(24) Qiao, P.; Harbottle, D.; Li, Z.; Tang, Y.; Xu, Z. Interactions of Asphaltene Subfractions in Organic Media of Varying Aromaticity. *Energy Fuels* **2018**, *32* (10), 10478−10485.

(25) Qiao, P.; Harbottle, D.; Tchoukov, P.; Wang, X.; Xu, Z. Asphaltene Subfractions Responsible for Stabilizing Water-in-Crude Oil Emulsions. Part 3. Effect of Solvent Aromaticity. *Energy Fuels* **2017**, *31* (9), 9179−9187.

(26) Mitra-Kirtley, S.; Mullins, O. C.; Ralston, C. Y.; Sellis, D.; Pareis, C. Determination of Sulfur Species in Asphaltene, Resin, and Oil Fractions of Crude Oils. *Appl. Spectrosc.* **1998**, *52* (12), 1522−1525.

(27) Waldo, G. S.; Mullins, O. C.; Penner-Hahn, J. E.; Cramer, S. P. Determination of the chemical environment of sulphur in petroleum asphaltenes by X-ray absorption spectroscopy. *Fuel* **1992**, *71* (1), 53−57.

(28) Wiltfong, R.; Mitra-Kirtley, S.; Mullins, O. C.; Andrews, B.; Fujisawa, G.; Larsen, J. W. Sulfur Speciation in Different Kerogens by XANES Spectroscopy. *Energy Fuels* **2005**, *19* (5), 1971−1976.

(29) Sinninghe Damste, J. S.; De Leeuw, J. W. Analysis, structure and geochemical significance of organically-bound sulphur in the geosphere: State of the art and future research. *Org. Geochem.* **1990**, *16* (4), 1077−1101.

(30) Payzant, J. D.; Montgomery, D. S.; Strausz, O. P. Novel terpenoid sulfoxides and sulfides in petroleum. *Tetrahedron Lett.* **1983**, *24* (7), 651−654.

(31) Ren, L.; Wu, J.; Qian, Q.; Liu, X.; Meng, X.; Zhang, Y.; Shi, Q. Separation and Characterization of Sulfoxides in Crude Oils. *Energy Fuels* **2019**, *33* (2), 796−804.

(32) Chacón-Patiño, M. L.; Rowland, S. M.; Rodgers, R. P. Advances in Asphaltene Petroleomics. Part 2: Selective Separation Method That Reveals Fractions Enriched in Island and Archipelago Structural Motifs by Mass Spectrometry. *Energy Fuels* **2018**, *32* (1), 314−328.

(33) Chacón-Patiño, M. L.; Rowland, S. M.; Rodgers, R. P. Advances in Asphaltene Petroleomics. Part 3. Dominance of Island or Archipelago Structural Motif Is Sample Dependent. *Energy Fuels* **2018**, *32* (9), 9106−9120.

(34) Chacón-Patiño, M. L.; Smith, D. F.; Hendrickson, C. L.; Marshall, A. G.; Rodgers, R. P. Advances in Asphaltene Petroleomics. Part 4. Compositional Trends of Solubility Subfractions Reveal that Polyfunctional Oxygen-Containing Compounds Drive Asphaltene Chemistry. *Energy Fuels* **2020**, *34* (3), 3013−3030.

(35) Strausz, O. P.; Torres, M.; Lown, E. M.; Safarik, I.; Murgich, J. Equipartitioning of Precipitant Solubles between the Solution Phase and Precipitated Asphaltene in the Precipitation of Asphaltene. *Energy Fuels* **2006**, *20* (5), 2013−2021.

(36) Chacón-Patiño, M. L.; Vesga-Martínez, S. J.; Blanco-Tirado, C.; Orrego-Ruiz, J. A.; Gómez-Escudero, A.; Combariza, M. Y. Exploring Occluded Compounds and Their Interactions with Asphaltene Networks Using High-Resolution Mass Spectrometry. *Energy Fuels* **2016**, *30* (6), 4550−4561.

(37) Juyal, P.; McKenna, A. M.; Fan, T.; Cao, T.; Rueda-Velásquez, R. I.; Fitzsimmons, J. E.; Yen, A.; Rodgers, R. P.; Wang, J.; Buckley, J. S.;

Gray, M. R.; Allenson, S. J.; Creek, J. Joint Industrial Case Study for Asphaltene Deposition. *Energy Fuels* **2013**, *27* (4), 1899−1908.

(38) Chacón-Patiño, M. L.; Blanco-Tirado, C.; Orrego-Ruiz, J. A.; Gómez-Escudero, A.; Combariza, M. Y. High Resolution Mass Spectrometric View of Asphaltene−SiO2 Interactions. *Energy Fuels* **2015**, *29* (3), 1323−1331.

(39) Loegel, T. N.; Danielson, N. D.; Borton, D. J.; Hurt, M. R.; Kenttämaa, H. I. Separation of Asphaltenes by Reversed-Phase Liquid Chromatography with Fraction Characterization. *Energy Fuels* **2012**, *26* (5), 2850−2857.

(40) Tapio, L.; Subramanian, S.; Simon, S.; Sjöblom, J. Solvent desorption of asphaltenes from solid surfaces. *J. Dispersion Sci. Technol.* **2017**, *38* (3), 355−360.

(41) Robb, D. B.; Covey, T. R.; Bruins, A. P. Atmospheric Pressure Photoionization: An Ionization Method for Liquid Chromatography-Mass Spectrometry. *Anal. Chem.* **2000**, *72* (15), 3653−3659.

(42) Kaiser, N. K.; Quinn, J. P.; Blakney, G. T.; Hendrickson, C. L.; Marshall, A. G. A Novel 9.4 T FTICR Mass Spectrometer with Improved Sensitivity, Mass Resolution, and Mass Range. *J. Am. Soc. Mass Spectrom.* **2011**, *22* (8), 1343−1351.

(43) Beu, S. C.; Blakney, G. T.; Quinn, J. P.; Hendrickson, C. L.; Marshall, A. G. Broadband Phase Correction of FT-ICR Mass Spectra via Simultaneous Excitation and Detection. *Anal. Chem.* **2004**, *76* (19), 5756−5761.

(44) Blakney, G. T.; Hendrickson, C. L.; Marshall, A. G. Predator data station: A fast data acquisition system for advanced FT-ICR MS experiments. *Int. J. Mass Spectrom.* **2011**, *306* (2), 246−252.

(45) Corilo, Y. E. *PetroOrg. N-18.3*; Florida State University, Omics LLC: Tallahassee, FL, 2014.

(46) Rytting, B. M.; Harper, M. R.; Edmond, K. V.; Merchant, S.; Zhang, Y.; Kilpatrick, P. K. Interfacial Phenomena of Purified Petroporphyrins and Their Impact on Asphaltene Interfacial Film Formation. *Energy Fuels* **2020**, *34* (5), 5444−5456.

(47) Rytting, B. M.; Harper, M. R.; Edmond, K. V.; Zhang, Y.; Kilpatrick, P. K. High-Purity Vanadyl Petroporphyrins: Their Aggregation and Effect on the Aggregation of Asphaltenes. *Energy Fuels* **2020**, *34* (1), 164−178.

(48) Schulze, M.; Lechner, M. P.; Stryker, J. M.; Tykwinski, R. R. Aggregation of asphaltene model compounds using a porphyrin tethered to a carboxylic acid. *Org. Biomol. Chem.* **2015**, *13* (25), 6984−6991.

(49) Hockaday, W. C.; Purcell, J. M.; Marshall, A. G.; Baldock, J. A.; Hatcher, P. G. Electrospray and photoionization mass spectrometry for the characterization of organic matter in natural waters: a qualitative assessment. *Limnol. Oceanogr.: Methods* **2009**, *7* (1), 81−95.

(50) Purcell, J. M.; Hendrickson, C. L.; Rodgers, R. P.; Marshall, A. G. Atmospheric pressure photoionization proton transfer for complex organic mixtures investigated by fourier transform ion cyclotron resonance mass spectrometry. *J. Am. Soc. Mass Spectrom.* **2007**, *18* (9), 1682−1689.

(51) Hertzog, J.; Carré, V.; Le Brech, Y.; Mackay, C. L.; Dufour, A.; Mašek, O.; Aubriet, F. Combination of electrospray ionization, atmospheric pressure photoionization and laser desorption ionization Fourier transform ion cyclotronic resonance mass spectrometry for the investigation of complex mixtures − Application to the petroleomic analysis of bio-oils. *Anal. Chim. Acta* **2017**, *969*, 26−34.

(52) McKenna, A. M.; Marshall, A. G.; Rodgers, R. P. Heavy Petroleum Composition. 4. Asphaltene Compositional Space. *Energy Fuels* **2013**, *27* (3), 1257−1267.

(53) Boduszynski, M. M. Composition of heavy petroleums. 1. Molecular weight, hydrogen deficiency, and heteroatom concentration as a function of atmospheric equivalent boiling point up to 1400.degree.F (760.degree.C). *Energy Fuels* **1987**, *1* (1), 2−11.

(54) Boduszynski, M. M.; Altgelt, K. H. Composition of heavy petroleums. 4. Significance of the extended atmospheric equivalent boiling point (AEBP) scale. *Energy Fuels* **1992**, *6* (1), 72−76.

(55) McKenna, A. M.; Blakney, G. T.; Xian, F.; Glaser, P. B.; Rodgers, R. P.; Marshall, A. G. Heavy Petroleum Composition. 2. Progression of the Boduszynski Model to the Limit of Distillation by Ultrahigh-Resolution FT-ICR Mass Spectrometry. *Energy Fuels* **2010**, *24* (5), 2939−2946.

(56) Chacón-Patiño, M. L.; Rowland, S. M.; Rodgers, R. P. The Compositional and Structural Continuum of Petroleum from Light Distillates to Asphaltenes: The Boduszynski Continuum Theory As Revealedby FT-ICR Mass Spectrometry. *The Boduszynski Continuum: Contributions to the Understanding of the Molecular Composition of Petroleum*; American Chemical Society: Washington, DC, 2018; Vol. 1282, pp 113−171.

(57) Nyadong, L.; Lai, J.; Thompsen, C.; LaFrancois, C. J.; Cai, X.; Song, C.; Wang, J.; Wang, W. High-Field Orbitrap Mass Spectrometry and Tandem Mass Spectrometry for Molecular Characterization of Asphaltenes. *Energy Fuels* **2018**, *32* (1), 294−305.

(58) Dong, X.; Zhang, Y.; Milton, J.; Yerabolu, R.; Easterling, L.; Kenttämaa, H. I. Investigation of the relative abundances of single-core and multicore compounds in asphaltenes by using high-resolution in-source collision-activated dissociation and medium-energy collision-activated dissociation mass spectrometry with statistical considerations. *Fuel* **2019**, *246*, 126−132.

(59) Podgorski, D. C.; Corilo, Y. E.; Nyadong, L.; Lobodin, V. V.; Bythell, B. J.; Robbins, W. K.; McKenna, A. M.; Marshall, A. G.; Rodgers, R. P. Heavy Petroleum Composition. 5. Compositional and Structural Continuum of Petroleum Revealed. *Energy Fuels* **2013**, *27* (3), 1268−1276.

(60) Murgich, J. Molecular Simulation and the Aggregation of the Heavy Fractions in Crude Oils. *Mol. Simul.* **2003**, *29* (6−7), 451−461.

(61) Chung, S.-H.; Violi, A. Peri-condensed aromatics with aliphatic chains as key intermediates for the nucleation of aromatic hydrocarbons. *Proc. Combust. Inst.* **2011**, *33* (1), 693−700.

(62) Abdul Jameel, A. G.; Khateeb, A.; Elbaz, A. M.; Emwas, A.-H.; Zhang, W.; Roberts, W. L.; Sarathy, S. M. Characterization of deasphalted heavy fuel oil using APPI (+) FT-ICR mass spectrometry and NMR spectroscopy. *Fuel* **2019**, *253*, 950−963.

(63) Elbaz, A. M.; Gani, A.; Hourani, N.; Emwas, A.-H.; Sarathy, S. M.; Roberts, W. L. TG/DTG, FT-ICR Mass Spectrometry, and NMR Spectroscopy Study of Heavy Fuel Oil. *Energy Fuels* **2015**, *29* (12), 7825−7835.

(64) Mitra-Kirtley, S.; Mullins, O. C.; Van Elp, J.; George, S. J.; Chen, J.; Cramer, S. P. Determination of the nitrogen chemical structures in petroleum asphaltenes using XANES spectroscopy. *J. Am. Chem. Soc.* **1993**, *115* (1), 252−258.

(65) Simon, S.; Nenningsland, A. L.; Herschbach, E.; Sjöblom, J. Extraction of Basic Components from Petroleum Crude Oil. *Energy Fuels* **2010**, *24* (2), 1043−1050.

(66) Zhang, L.-L.; Wang, C.-L.; Zhao, Y.-S.; Yang, G.-H.; Su, M.; Yang, C.-H. Speciation and quantification of sulfur compounds in petroleum asphaltenes by derivative XANES spectra. *Journal of Fuel Chemistry and Technology* **2013**, *41* (11), 1328−1335.

(67) Nahid Siddiqui, M. Infrared Study of Hydrogen Bond Types in Asphaltenes. *Pet. Sci. Technol.* **2003**, *21* (9−10), 1601−1615.

(68) Mullins, O. C. The Modified Yen Model. *Energy Fuels* **2010**, *24* (4), 2179−2207.

(69) Ballard, D. A.; Chacón-Patiño, M. L.; Qiao, P.; Roberts, K. J.; Rae, R.; Dowding, P. J.; Xu, Z.; Harbottle, D. *Data associated with 'Molecular Characterization of Strongly and Weakly Interfacially Active Asphaltenes by High-Resolution Mass Spectrometry'*, University of Leeds, 2020. [Dataset] DOI: 10.5518/883.